frontiers | Frontiers in Marine Science

TYPE Original Research
PUBLISHED 22 February 2023
DOI 10.3389/fmars.2023.1052044

Check for updates

OPEN ACCESS

EDITED BY
Pengfei Xue,
Michigan Technological University,
United States

REVIEWED BY
Matthew Buckley Alkire,
University of Washington, United States
Juan Jose Munoz-Perez,
University of Cádiz, Spain
Jianzhong Ge,
East China Normal University, China

*CORRESPONDENCE
Alexander Osadchiev
osadchiev@ocean.ru

SPECIALTY SECTION
This article was submitted to Coastal Ocean Processes, a section of the journal Frontiers in Marine Science

RECEIVED 23 September 2022
ACCEPTED 10 February 2023
PUBLISHED 22 February 2023

CITATION
Rogozhin V, Osadchiev A and Konovalova O (2023) Structure and variability of the Pechora plume in the southeastern part of the Barents Sea. *Front. Mar. Sci.* 10:1052044. doi: 10.3389/fmars.2023.1052044

COPYRIGHT
© 2023 Rogozhin, Osadchiev and Konovalova. This is an open-access article distributed under the terms of the Creative Commons Attribution License (CC BY). The use, distribution or reproduction in other forums is permitted, provided the original author(s) and the copyright owner(s) are credited and that the original publication in this journal is cited, in accordance with accepted academic practice. No use, distribution or reproduction is permitted which does not comply with these terms.

Structure and variability of the Pechora plume in the southeastern part of the Barents Sea

Vladimir Rogozhin[1,2], Alexander Osadchiev[1,3]* and Olga Konovalova[2]

[1]Shirshov Institute of Oceanology, Russian Academy of Sciences, Moscow, Russia, [2]Marine Research Center at Lomonosov Moscow State University, Moscow, Russia, [3]Moscow Institute of Physics and Technology, Dolgoprudny, Russia

The Pechora River forms the large Pechora River plume in the southeastern part of the Barents Sea (also called the Pechora Sea). Many previous works addressed water masses in the Barents Sea, however, the Pechora plume received relatively little attention, therefore, many basic aspects of its structure and variability remain unknown. In this study, we focus on spreading of the Pechora plume in the Pechora Sea during ice-free periods. Based on the extensive *in situ* measurements and satellite observations, we describe the dependence of area and spatial characteristics of the Pechora plume on wind forcing, river discharge rate, and spring ice conditions. We reveal three general types of Pechora plume spreading, which are determined by the external forcing conditions. Joint analysis of a large set of *in situ* and satellite data provided opportunity to study the variability of the Pechora plume on the synoptic, seasonal, and interannual time scales. We reveal regular advection of the Pechora plume through the Kara Strait into the Kara Sea. In addition, we describe formation of a significant area of increased salinity within the Pechora plume formed during wind-induced coastal upwelling events. The results of this research are of key importance for understanding the physical, biological, and geochemical processes in the Pechora Sea and the adjacent areas of the Barents and Kara seas.

KEYWORDS

river plume, surface salinity, wind forcing, synoptic variability, seasonal variability, coastal upwelling, Barents Sea, Pechora Sea

1 Introduction

The Barents Sea is a marginal sea in the western part of the Arctic Ocean (Figure 1). The hydrological regime of the Barents Sea is determined by the inflow of, first, saline and warm water from the North Atlantic and, second, low-saline and cold water from the central part of the Arctic Ocean (Smedsrud et al., 2010; Smedsrud et al., 2013). The Norwegian Coastal Current is the main freshwater source for the Barents Sea (Skagseth

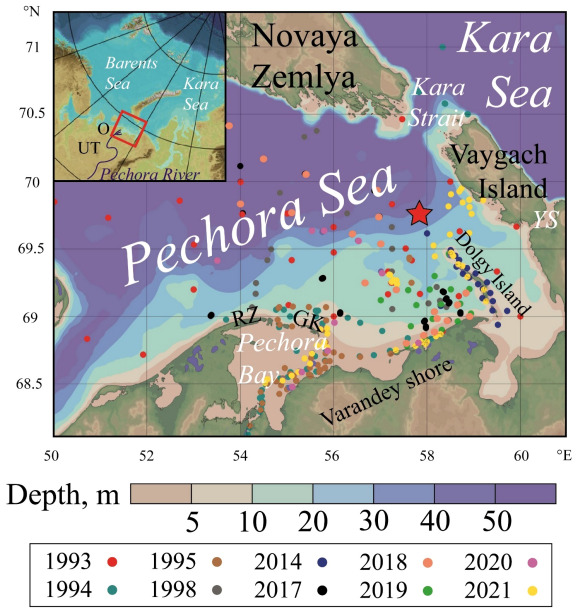

FIGURE 1
Bathymetry of the Pechora Sea, locations of CTD stations (colored circles) and location of the mooring station (red star) analyzed in this study. RZ denotes the Russkiy Zavorot peninsula, GK denotes the Gulyaevskie Koshki archipelago, which bound the Pechora Bay; KS denotes the Kara Strait, YS denotes the Yugorsky Strait, which connect the Pechora and Kara seas. The inset demonstrates location of the Pechora Sea (red rectangle) in the Western Arctic; the Pechora River and the river gauge stations Oksino (O) and Ust-Tsilma (UT) (green squares). The bathymetric data was taken from the International Bathymetric Chart of the Arctic Ocean (IBCAO) (Jakobsson et al., 2012).

et al., 2011), while river runoff into the Barents Sea is relatively low (260 km^3 annually) and limitedly affects regional hydrological processes. The important exception is the southeastern part of the Barents Sea (which is also called the Pechora Sea) (Figure 1) (Nikiforov et al., 2005a). It receives large runoff from the Pechora River with average annual discharge of 150 km^3 (Gordeev et al., 1996; Magritsky et al., 2017). The Pechora River is the 6th largest river in the Arctic in terms of annual discharge after the Yenisei (620 km^3), Lena (530 km^3), Ob (430 km^3), Mackenzie (320 km^3), and Yukon (200 km^3) rivers. The annual discharge of the Pechora River accounts for 3.5% of total annual river runoff to the Arctic Ocean (Haine et al., 2015).

The Barents Sea is among the most studied among the Arctic seas (e.g., Loeng et al., 1997; Dankers and Middelkoop, 2008; Arthun et al., 2011; Drinkwater, 2011; Boitsov et al., 2012; Smedsrud et al., 2013; Lind et al., 2018; Skagseth et al., 2020; Liu et al., 2022). However, its shallow southeastern part received much less attention. Studies of the Pechora Sea mainly described general oceanographic conditions in this region; most of them were based on 1-2 local field surveys (Loeng, 1991; Ilyin and Matishov, 1992; Adrov and Denisenko, 1996; Byshev et al., 2001; Nikiforov et al., 2005a; Nikiforov et al., 2005b; Mokhova et al., 2019). In particular, we are not aware of any study considering the Pechora plume as an individual water mass. Therefore, even basic aspects of its spatial and vertical structure, as well as temporal variability still remain unknown.

Several papers describe the significant influence of the Pechora plume on plankton communities in the Pechora Sea (Lee et al., 2003; Dvoretsky and Dvoretsky, 2013; Gerasimova et al., 2019; Usov et al., 2019). In addition, rapid changes in thermohaline characteristics of the bottom layer in the shallow Pechora Sea, which are also associated with variability of the Pechora plume, strongly affect local macrozoobenthos communities. These communities are an important component of the forage base of the Atlantic walrus subspecies that is included in the Red Book of the Russian Federation (state document established for documenting rare and endangered species) (Dahle et al., 1998; Denisenko et al., 2000; Denisenko et al., 2003; Denisenko et al., 2019a; Denisenko et al., 2019b). In particular, Denisenko et al. (2019a) demonstrated that macrozoobenthos communities experience the greatest changes during freshet period, which highlights the role of the Pechora plume.

This paper analyzes the extensive data set of *in situ* measurements acquired in the Pechora Sea in 1993-2021. Based on these data, which is also supported by thermal satellite imagery, we describe (1) the vertical and spatial structure of the Pechora plume; (2) synoptic, seasonal, and inter-annual variability of the Pechora plume; (3) response of the Pechora plume to wind forcing, river discharge variability, and spring sea ice melting. To the extent of our knowledge, this paper provides the first thorough description of structure and variability of the Pechora plume. This work continues our previous studies of large river plumes in the Eurasian Arctic including the Ob-Yenisei plume in the Kara Sea (Osadchiev et al., 2017; Osadchiev et al., 2019; Osadchiev et al., 2021a; Osadchiev et al., 2021c), the Khatanga, Lena, Indigirka and Kolyma plumes in the Laptev and East-Siberian seas (Osadchiev et al., 2020b; Osadchiev et al., 2020c; Spivak et al., 2021; Osadchiev et al., 2021b), the large-scale freshwater transport in the Eastern Arctic (Osadchiev et al., 2020a; Osadchiev, 2021). Note that in this paper, we describe the response of a medium-size river plume (with area ~10 000 km^2) to external forcing, while our previous studies of the Arctic River plumes were focused on large river plumes (with area ~100 000 km^2).

2 Study area, data, and methods

2.1 Study area

The Pechora Sea is a shelf marginal sea located between the continental coast in the south, the Vaygach Island and Novaya Zemlya in the east, and the Kolguev Island in the west (Figure 1). The northern boundary of the sea is determined by the line between the Kolguev Island and cape Cherniy at the northern shore of Novaya Zemlya. The Pechora Sea in connected with the central part of the Barents Sea in the northwest and with the Kara Sea in the east by the narrow Yugorsky and Kara straits (also called as the Kara Gates Strait). The Pechora Sea is small (with area of 81 000 km^2)

and shallow (with average depth of 6 m). The Pechora Bay located in the southern part of the Pechora Sea is a large choked estuary of the Pechora River (Figure 1). The Pechora Bay is bounded by the Russkiy Zavorot peninsula and the Gulyaevskie Koshki archipelago. Narrow and shallow straits between the islands of the archipelago hinder water exchange between the Pechora Bay and the Pechora Sea, which is a typical feature for choked estuaries (Osadchiev, 2017; Zavialov et al., 2020). Tidal circulation in the Pechora Sea is relatively low; the average tidal amplitude is equal to 1 meter (Nikiforov et al., 2005a). Tidal wave enters the Pechora Bay from the north through the Gulyaevskie Koshki archipelago, which strongly reduces the intensity of the tidal forcing in the bay. The Pechora Sea is covered by ice from October – November to May – June.

2.2 Data

In order to study the structure and variability of the Pechora plume, we analyzed *in situ* measurements of temperature and salinity performed during 12 oceanographic surveys in the Pechora Sea in 1993-2021. Data from the most recent surveys (6 cruises in 2017-2021) were not described and discussed before; data from 3 cruises in 1993-1995 were taken from the World Ocean Database (Boyer et al., 2018), data from two more cruises in 1998 and 2014 were taken from Vedernikov et al. (2001) and Usov et al. (2019), respectively. The information about the field surveys is summarized in Table 1. Thermohaline measurements were performed using various CTD profilers (Neil Brown MK3B; YSI Castaway; RBR Concerto) and were carried out from June to September, covering both the spring-summer freshet period and the summer-autumn drought period. The resulting extensive data set (more than 150 CTD stations) provides very good spatial and temporal coverage of the study area (colored circles in Figure 1). Due to usage of different CTD profilers in different field surveys, we estimate the accuracy of temperature and salinity measurements in the resulting data set as 0.05°C and 0.05 psu according to their intercalibration at deep stations.

TABLE 1 Periods and research vessels of 12 oceanographic surveys and a mooring station analyzed in this paper.

Period	Research vessel	Data reference
14-23.07.1993	Dalnie Zelentsy	World Ocean Database
23-27.07.1994	Kartesh	World Ocean Database
10-17.07.1995	Kartesh	World Ocean Database
10-20.08.1998	Sergey Vavilov	Vedernikov et al., 2001
1.07-1.11.2002	Mooring station	This paper
13-14.07.2014	Dalnie Zelentsy	Usov et al., 2019
23-27.07.2017	Kartesh	This paper
18-23.07.2018	Kartesh	This paper
21-25.06.2019	Kartesh	This paper
24.07.2019	Kartesh	This paper
19.07-25.07.2020	Kartesh	This paper
7-20.07.2021	Kartesh	This paper

In addition to field measurements, we analyzed optical and thermal satellite images of the Pechora Sea taken by MODIS Terra/Aqua, NOAA-20/VIIRS, and Suomi NPP/VIIRS in 2000–2021 on a daily basis with spatial resolution of 250 m. In addition, in certain cases we analyzed Landsat-8 optical and thermal satellite images with spatial resolution of 30 m. Satellite data were provided by the United States Geological Survey (USGS) (http://earthexplorer.usgs.gov). The Pechora River discharge measurements analyzed in this study were acquired from two most downstream gauge stations located in Ust-Tsilma and Oksino (green squares in the inset in Figure 1). Wind forcing conditions in the study area were examined using Climate Forecast System Reanalysis (CFSR) atmospheric reanalysis with hourly temporal resolution and 0.5° spatial resolution (Saha et al., 2010; Saha et al., 2014). In order to assess the response of the Pechora plume to wind forcing conditions, wind was averaged over the area 54 – 60°E, 68.5 – 69.5°N. This area is commonly covered by the Pechora plume according to *in situ* and satellite imagery; therefore, this spatial averaging could be applied to study spreading of the Pechora plume. This methodology was used in our previous studies (Osadchiev, 2017; Osadchiev et al., 2020a; Osadchiev et al., 2021c). The sea ice data retrieved from satellite products were downloaded from the web repository of the Arctic and Antarctic Research Institute (http://old.aari.ru/odata/_d0015.php?mod=1).

2.3 River discharge

The annual runoff of the Pechora River varies from 120 to 200 km^3 (Figure 2). The majority of the Pechora annual runoff enters the sea during the freshet period in May-July (Dankers and Middelkoop, 2008; Magritsky et al., 2017) (Figure 3). The long-term averaged peak discharge rate during the freshet period is equal to 27 000 m^3/s, while the maximal registered discharge was 39 200 m^3/s in 1991 (Magritsky et al., 2017). During winter-spring drought, the discharge decreases to 500-750 m^3/s.

Figure 3 demonstrates the daily variability of the Pechora River discharge during ice-free period in 2017-2021 with indication of periods of the analyzed field surveys. During 2017-2021, the most detailed surveys of the Pechora Sea were conducted among those analyzed in this paper. Among these five years, the largest discharge rates were observed in 2017. Maximal discharge values in 2017 were equal to 30 000 - 36 000 m^3/s within one prominent peak during the summer freshet, which lasted for 1.5 months from the early June to the middle of July. The discharge variability in 2020 also had one distinct peak with lower values than in 2017 (30 000 m^3/s). The freshet period in 2020 started two weeks earlier than in 2017, in the middle of May, and lasted only a month till the middle of June. In 2018 and 2019, maximal discharge rates (22 000-23 000 m^3/s) were significantly lower than those in 2017 and 2020. The freshet period in 2018 and 2019 lasted during two months from the middle of May till the middle of July with several flow peaks. As a result, the total runoff volume of the Pechora River during ice-free period in 2017

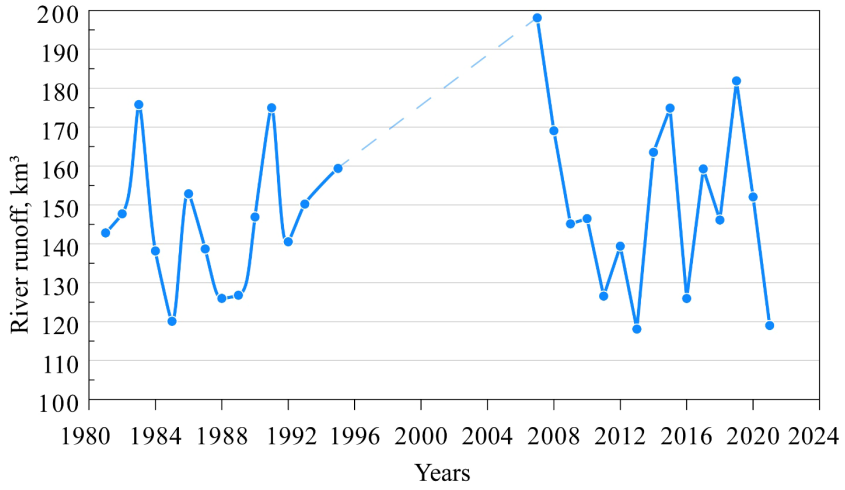

FIGURE 2
Inter-annual variability of the Pechora River runoff in 1981-1995 and 2006-2021.

(90 km^3) and 2020 (86 km^3) was greater than in 2018 (75 km^3). On the opposite, total runoff in May – October in 2019 (92 km^3) was greater than those in 2017 and 2020 due to relatively high discharge rates during the drought period. A significantly smaller total runoff of the Pechora River was observed in 2021 (67 km^3), due to short freshet period (from the middle of May till the middle of June) and low peak discharge values, which were about 1.5 times less than the maximal values in 2017 and 2020.

2.4 Ice conditions

The ice coverage in the Pechora Sea starts to form in late October – early November. Ice steadily expands northward from the continental coast and covers the majority of the sea by the end of December. Intense ice melting starts in May and the sea becomes completely free of ice in late June – early July, albeit during certain warm years it happens a month earlier (Zabolotskikh and Balashova, 2021). The longest presence of ice occurs in the eastern part of the sea near the Vaygach Island and the Yugorsky Strait.

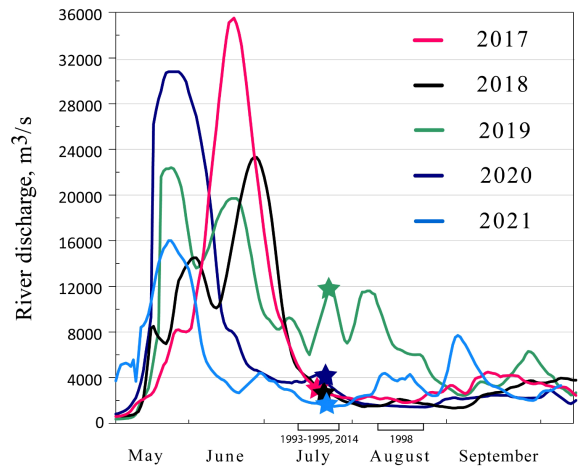

FIGURE 3
Daily variability of the Pechora River discharge during ice-free period in 2017-2021. Periods of surveys in 2017-2021 are indicated by color stars. Periods of surveys in 1993-1995, 1998 and 2014 are indicated by black rectangles on the bottom axis.

In this study, we analyze ice coverage during the freshet season due to possible contribution of ice melting (in addition to river discharge) to formation of the freshened surface layer in the Pechora Sea. In most cases, this contribution is insignificant because of the following reasons. First, during warm years, the majority of the Pechora Sea is covered by thin ice (10-30 cm), which completely melts by the middle of May. In these years a relatively small volume of melt water (1-2 km^3) completely mixes with saline seawater during at least several weeks before the start of the freshet period. Second, during certain years, sea ice is actively advected by wind from the Pechora Sea to the central part of the Barents Sea. This advection in spring results in low flux of melt water to surface layer in the Pechora Sea. Analysis of satellite ice maps of the Pechora Sea for 22 years (from 1999 to 2021) showed that only in 7 cases (1999, 2001, 2002, 2003, 2013, 2014, and 2018) significant volume of sea ice was present in the Pechora Sea by the beginning of the spring freshet of the Pechora River. During these years, melt water (10-12 km^3) could significantly contribute to the formation of the freshened surface layer in the Pechora Sea, and, therefore, artificially increase the volume and area of the Pechora plume. The precise estimation of total volume of melt water during these years is beyond this paper due to large uncertainties of estimation of ice thickness, especially in spring and summer during melting period (Kurtz and Markus, 2012; Mu et al., 2018a; Mu et al., 2018b).

2.5 Comparison of satellite and *in situ* data

Analysis of satellite images of the Pechora Sea provides opportunity to significantly extend spatial and temporal coverage

of available *in situ* measurements and to improve the understanding of variability of area of the Pechora plume. Nevertheless, usage of satellite data for detecting large river plumes requires verification against synchronous *in situ* measurements, otherwise straightforward usage of satellite data could be misleading (Frey and Osadchiev, 2021).

In this study, we do not use optical satellite data to detect spreading area of the Pechora plume, because these data is effective for detection only small river plumes with small residence time (hours and days) of turbid freshwater within a plume (Osadchiev and Zavialov, 2020). Large river plumes with high residence time (weeks and months) demonstrate elevated turbidity only in vicinity of river estuaries and deltas, while turbidity of far-field parts of large plumes is similar to that in the ambient saline sea. Satellite-derived sea surface temperature, on the opposite, is a stable marker of river plumes in the Arctic Ocean. Due to a significant difference in temperatures of river discharge and ambient seawater (up to 10-12° C in June – August), the Pechora plume is detected in thermal satellite images as an area of increased sea surface temperature. Generally, this area has a distinct outer front, which is typically manifested at satellite images by sharp temperature gradient. Note that specific temperature contours (as compared to maximal temperature gradient) do not provide stable border detection due to steady seasonal cooling of the Pechora plume.

In order to verify that this thermal frontal zone indeed coincides with the outer boundary of the Pechora plume (determined by reduced salinity), we compared *in situ* measurements in the Pechora Sea acquired in 2018, 2019, 2020, and 2021 with the synchronous satellite images. Figure 4 demonstrates that location of the Pechora plume border, determined from satellite images, shows very good agreement with the plume border determined from synchronous salinity measurements. It should be noted that we used visual detection of the plume border at satellite imagery, which has a certain human bias. However, due to large temperature

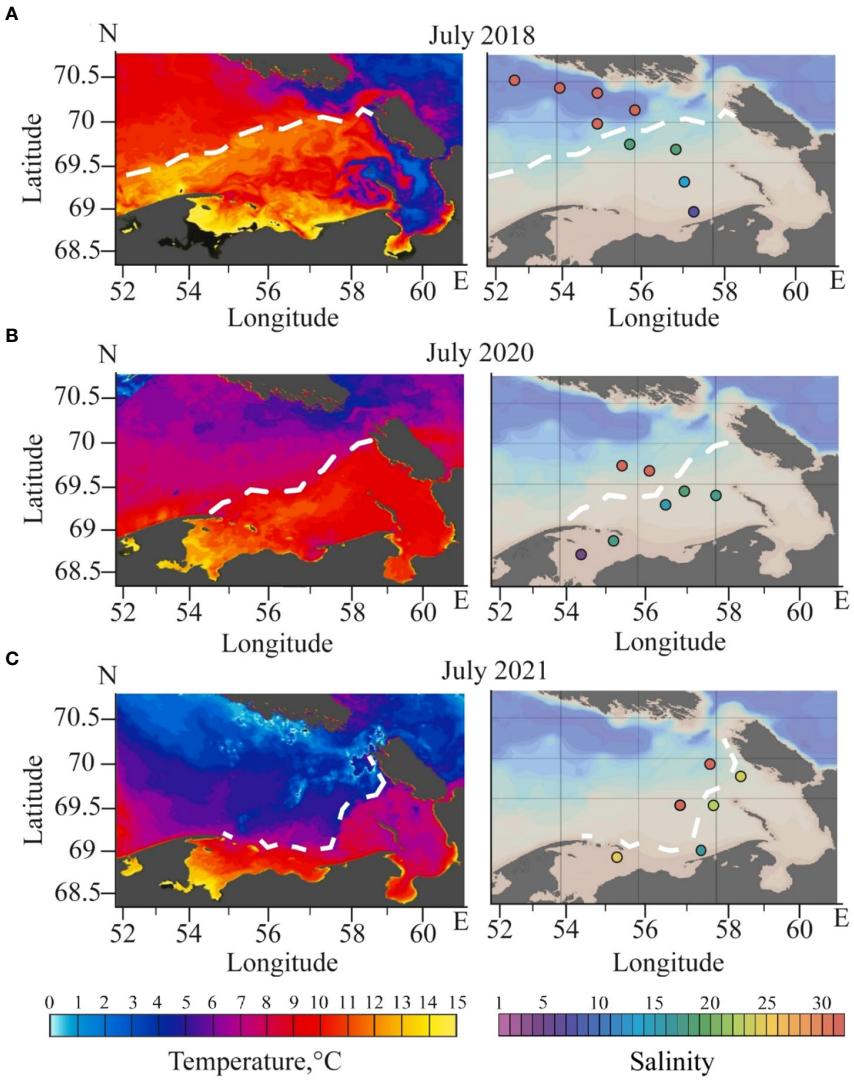

FIGURE 4
Locations of the Pechora plume border (white dashed lines) detected by satellite thermal imagery (left) and in situ salinity data (right) on 21 July 2018 **(A)**, 19 July 2020 **(B)**, and 7 July 2021 **(C)**. Surface salinity values acquired from in situ measurements are shown by color dots.

difference between the Pechora plume and saline seawater, we believe that the applied visual approximation provides correct results for this study.

3 Results

3.1 Vertical structure of the Pechora plume

The vertical structure of the Pechora River plume was investigated using *in situ* data obtained during the surveys of RV Kartesh and Dalnie Zelentsy in July-August 1993-1995, 2014, 2017-2021. The isohaline of 25 is regarded as the outer boundary of the Pechora plume, similarly to other large river plumes in the Arctic Ocean (e.g., Ob-Yenisei, Lena, Khatanga) (Osadchiev et al., 2020a; Osadchiev et al., 2021a; Osadchiev et al., 2021b). In case of the Pechora plume, *in situ* measurements demonstrate that both horizontal and vertical salinity gradients are observed at the isohalines of 23-27 (Figures 5, 6).

Figure 5 shows typical plots of vertical salinity distribution in different parts of the Pechora Sea. In all these regions, salinities in the surface layer (till the depths of 5-15 m) shows significant variability associated with presence or absence of the Pechora plume. The Pechora plume is regularly registered in the central part of the Pechora Sea (Figure 5A) and near the Vaygach Island (Figure 5B), on the other hand, the plume was absent in these regions during many field surveys. In the central part of the Pechora Sea, in case of presence of the Pechora plume, surface salinity is 10-20 followed by sharp salinity gradient; while in case of absence of the plume, salinity is almost homogenous from surface to bottom and is equal to 32-33 (Figure 5A). Depth of the plume in the central part of the sea generally is 4-5 m; however, in July 2020, depth increased to 10-12 m in response to a significant increase in the plume area. Similarly, near the Vaygach Island surface salinity is 24-25 in case of presence of the plume (7-8 m deep) and is 31-32 in case of its absence (Figure 5B).

Areas near the Dolgy Island (Figure 5C), Varandey shore (Figure 5D), and Pechora Bay (Figure 5E) demonstrate reduced surface salinity (15-25) due to almost constant presence of the plume. Vertical salinity gradients generally are much smaller at these areas, as compared to the central part of the sea. Higher values of surface salinity (27-28) were rarely recorded only near the

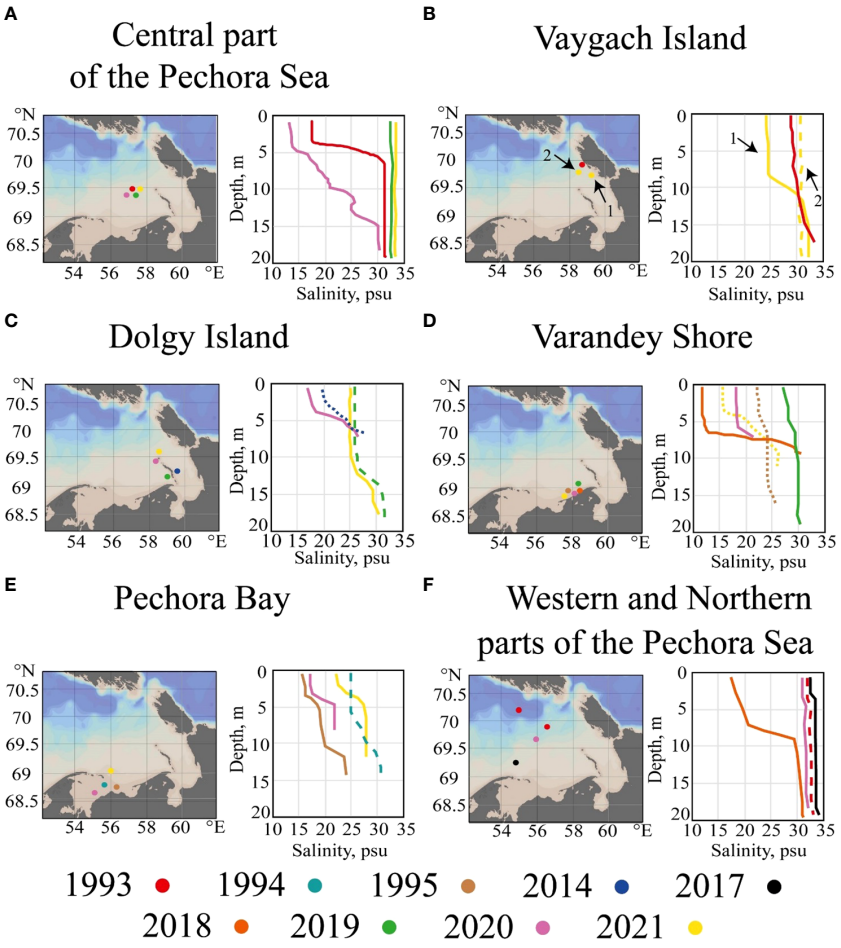

FIGURE 5
Typical vertical salinity structure in the central part of Pechora Sea **(A)**, near Vaygach Island **(B)**, Dolgy Island **(C)**, Varandey shore **(D)**, in the Pechora Bay **(E)**, western and northern parts of the Pechora Sea **(F)** in July-August 1993-1995, 2014, 2017-2021. We used two types of lines (dashed and dotted) for better visibility in case of overlapping stations or matching colors.

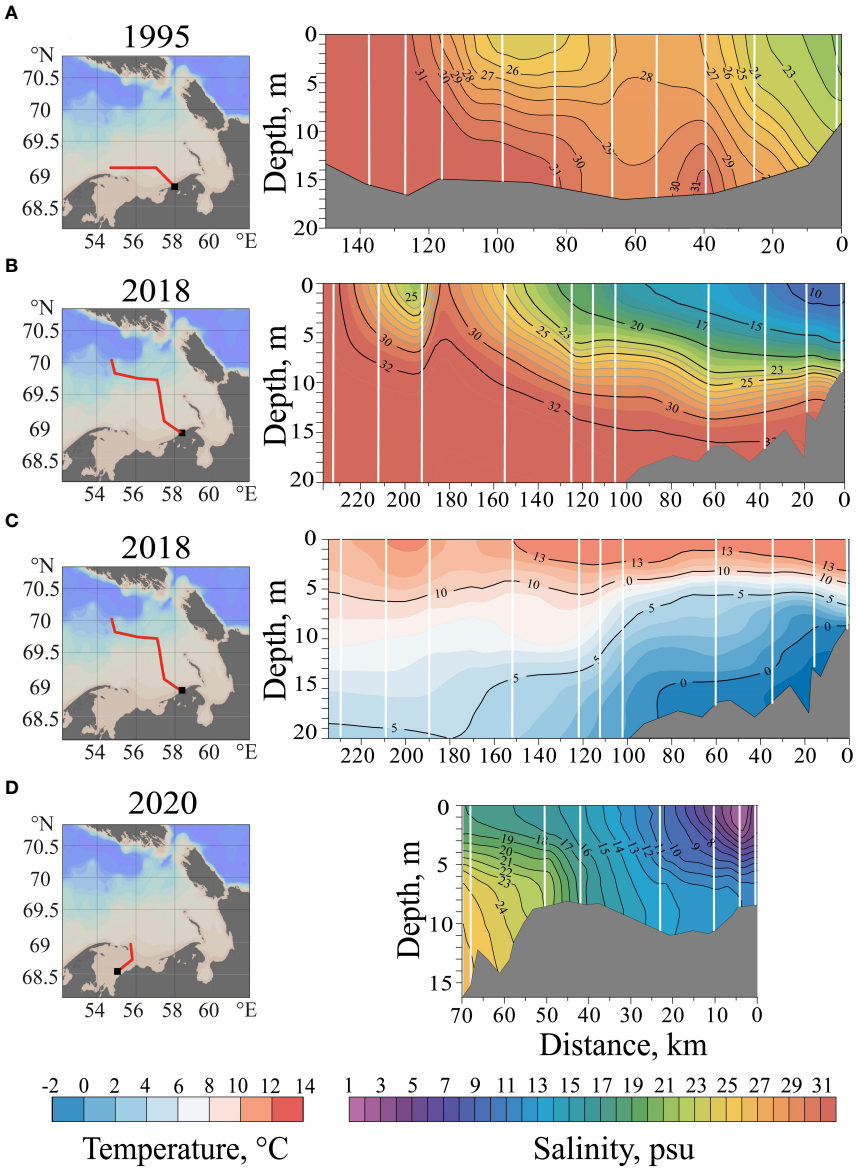

FIGURE 6
The vertical salinity structure along the Varandey shore on 9-17 July 1995 **(A)**, in the central part of the Pechora Sea on 18-23 July 2018 **(B)**, in the Pechora Bay on 16-19 July 2020 **(D)**. The vertical temperature structure in the central part of the Pechora Sea on 18-23 July 2018 **(C)**. Black squares at the left insets shows location of beginning point of the sections. The bathymetric data in 1995 were taken from the International Bathymetric Chart of the Arctic Ocean (IBCAO) (Jakobsson et al., 2012); the bathymetric data in 2018 and 2020 were taken from shipboard echo sounding.

Varandey shore (Figure 5D). The Pechora plume generally is not registered in the western and northern parts of the Pechora Sea, except periods of the significant increase in the plume area as was observed in July 2018 (Figure 5F). In this case, surface salinity decreases to 15-20 and the plume depth is 7-8 m.

Thermohaline measurements along sections at different parts of the study area provide information about spreading area and vertical structure of the Pechora plume during the periods of field surveys (Figure 6). Figure 6A shows the vertical distribution of salinity along the section from the Russkiy Zavorot Peninsula to the Varandey shore in July 1995. The most freshened waters are located near the Varandey shore with salinities ranging from 20 to 23. This water mass is associated with the alongshore buoyancy current carrying plume waters from the Pechora Bay to the east along the Varandey shore. The width of this current is 20-25 km, and it occupies the entire water column from surface to bottom (7-10 m). During the freshet period, salinity within this current decreases to 10-15 (Figure 5D). Another area of reduced salinity (25-26) as compared to typical sea salinity (30-32), is observed northeastward from the Russkiy Zavorot Peninsula indicating the source of the alongshore freshened current near the Pechora Bay (Figure 6A).

Figures 6B and 6C demonstrate the vertical salinity and temperature structure along the section from the Varandey shore to the northern part of the Pechora Sea. These measurements demonstrate wide spreading of the Pechora plume in July 2018, which is registered along large segments of the transect. Surface

salinity within the plume increases from 10-16 near the Varandey shore to 24-25 at the distance of 100-150 km from the Pechora Bay and the Varandey shore. Surface temperature along this transect decreases from 14 to 10-12°C. Depth of the plume is stable and equal to 8-12 m.

The Pechora Bay is the area of initial mixing of the Pechora River discharge and saline seawater. The vertical salinity structure in the Pechora Bay in July 2020 is shown in Figure 6D. The lowest salinity values (2-15) from surface to bottom are observed near the Pechora River Delta during the freshet period. Surface and bottom salinities increase to 17-18 and 23-25, respectively, in the northern part of the Pechora Bay indicating the inflow of saline seawater to the bay.

3.2 Spatial structure of the Pechora plume

Based on salinity measurements and satellite data, we reconstructed location of the isohaline of 25 in the surface layer during 10 oceanographic surveys in 1993-2021 (Figure 7). Among them, only several oceanographic surveys covered the entire study area at the Pechora Sea, while the majority of surveys were focused on certain parts of this area. Due to this fact, locations of the plume boundary were reconstructed from satellite thermal data verified by synchronous *in situ* measurements. We presume that the reconstructed plume areas represent the plume during the periods of the surveys. Also in Figure 7 we show average wind forcing conditions during the periods of field surveys.

The reconstructed area and position of the Pechora plume demonstrates significant inter-annual variability (Figure 7). In 1993 (14-23 July), 1994 (23-27 July), 1995 (10-17 July), 1998 (10-20 August), and 2019 (25 June and 24 July), the Pechora plume had the smallest area, it occupied the Pechora Bay and the area along the Varandey shore. In these years, oceanographic surveys were carried out either in mid-July, i.e., during or immediately after the freshet period, or in mid-August, i.e. much later the freshet period. The shape of the plume demonstrates that the initial impulse of the river jet decays within the semi-isolated Pechora Bay and the plume was spreading eastward from the estuary as an alongshore gravity current (Polonsky, 2012). Localization of the Pechora plume near the Pechora Bay was caused by the joint influence of relatively early freshet river discharge and strong northwestern and western wind forcing. In particular, in June 2019, wind speed at the study area was 10-15 m/s shortly before the field survey, which caused intense mixing of the Pechora plume, followed by moderate western winds (8-9 m/s), which localized the plume near the estuary.

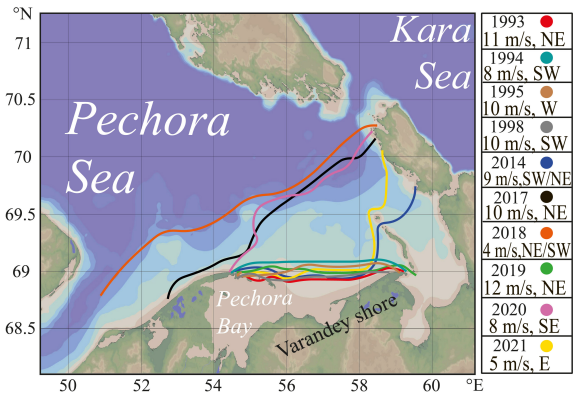

FIGURE 7
Locations of the isohaline of 25 in the surface layer in the Pechora Sea, which represents the Pechora plume border, detected by in situ measurements during field surveys and supported by satellite data. Average wind forcing conditions during the periods of field surveys are shown in the inset.

In 2014 (13-14 July) and 2021 (07-20 July), the Pechora plume extended further eastward and occupied the area between the Dolgy and Vaygach islands. Plume spreading during these periods occurred under the influence of low winds (< 5 m/s) with variable direction, which resulted in further propagation of the alongshore gravity current. In particular, in 2021 wind forcing was low from the freshet peak in the middle of June till the period of field survey in the middle of July, therefore, the plume retained its area covered during the freshet period. In addition, in 2014 the Pechora plume was inflated due to meltwater contribution as a result of intense sea ice melting, which occurred in the area between the Dolgy and Vaygach islands. This process artificially increased the area of the Pechora plume.

In 2017 (23-27 July), 2018 (18-23 July), and 2020 (19-25 July) the Pechora plume had the largest area and covered the whole region between the Pechora Bay and the Vaygach Island. During all these years, the *in-situ* measurements were performed during and shortly after the peak freshet period (Figure 3), and the plume was spreading under low wind forcing (< 5 m/s). The largest registered plume area in 2018 was caused by the additional contribution to freshwater volume from ice melting shortly before and during the field survey.

3.3 Variability of area of the Pechora plume

After the performed validation of satellite data against *in situ* measurements described in section 2.5, we could use satellite thermal images to estimate area of the Pechora plume and assess its temporal variability in response to local wind forcing. For this purpose, we used daily MODIS Terra/Aqua images acquired during relatively long cloud-free period from late June to late July in 2019 (Figure 8). On 28 June, the Pechora plume occupied relatively narrow stripe along the continental shore in the southern and southeastern parts of the Pechora Sea (Figure 8A). Moderate northwestern and western wind (8-11 m/s), which dominated in the study area on 12-26 June, pressed the Pechora plume southward to the Varandey shore due to the resulting Ekman transport. However, low wind forcing (< 3 m/s) on 27 June – 2 July with a short-term period of strong southeastern wind (up to 10 m/s) on 30 June significantly increased area of the Pechora plume and moved its border northward by 100-120 km, which is distinctly visible at satellite image acquired on 3 July (Figure 8B). Strong eastern and northeastern wind (up to 12-15 m/s) during 3-13 July caused intense mixing of the Pechora plume with subjacent saline seawater. As a result, the plume area significantly decreased and,

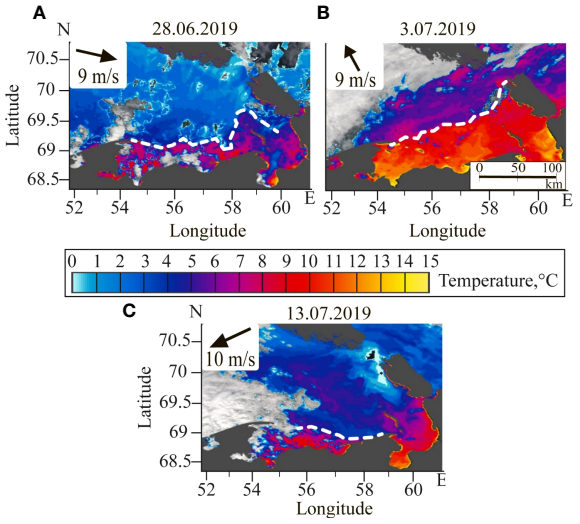

FIGURE 8
Satellite-derived sea surface temperature in the Pechora Sea on 28 June **(A)**, 3 July **(B)**, 13 July **(C)** 2019 acquired by MODIS Terra/Aqua. Locations of the Pechora plume border is indicated by white dashed lines. Dark grey color indicates land, white color indicates cloud coverage of the study area. Wind directions and velocities averaged during two days preceding the satellite image are shown in the insets.

by 13 July, the plume remained only within the Pechora Bay (Figure 8C). During the next 10 days, wind forcing was moderate (4-8 m/s) with variable direction, therefore, the Pechora plume restored its area.

To study synoptic variability of the Pechora plume, we analyzed a series of daily thermohaline measurements, collected at the mooring station located northward from the Dolgy Island (indicated by red star in Figure 1). The measurements were performed in the surface layer (at the depth of 3.5 m) from 19 July to 1 October 2002 (Figure 9). During 2.5 months of measurements, three periods of reduced surface salinity (indicated by green lines in Figure 9) were registered. During these periods, salinity abruptly decreased from 31-33 (typical for saline seawater) to 21-25, which was caused by advection of the Pechora plume to the point of measurements. During the first and the second periods in July and August, temperatures synchronously increased by 4-5°C indicating warm water of the Pechora plume. Atmospheric heating and cooling affected temperature of the Pechora plume, it changed from 7-8°C during the first period in mid-July to 10-11°C during the second period in late-August. However, temporal scale of these changes is much greater than synoptic changes of sea surface temperature registered at the mooring station related to changes in position of the Pechora plume. During the third period in late September, no increase of temperature was observed. Due to already very low air temperatures, atmospheric cooling significantly reduced the plume temperature, so the thermal difference between the plume and the ambient sea vanished. This feature is also clearly visible at thermal satellite imagery, so in this study we analyze only images acquired in June-August for detection of the Pechora plume.

The joint analysis of this series of thermohaline data, satellite images, and wind data allowed us to estimate the temporal scale of response of the Pechora plume to synoptic wind forcing variability. The first period of reduced salinity at the mooring station was observed on 20-31 July (Figure 9). Strong northeastern wind (5-10 m/s) prevailed over the Pechora Sea on 13-20 July, which caused northwestern propagation of the Pechora plume and its advection to the mooring station area. As a result, surface salinity at the station decreased to 23-25 in the middle of July. Low (4-5 m/s) and variable wind forcing on 21-27 July resulted in stable position of the plume. The subsequent strong western wind (8-12 m/s), which dominated from 27 July to 3 August, caused southward advection of the plume. Surface salinity at the mooring station increased to 30-32 on 31 July, i.e., 4 days after the change in wind conditions. On 4-12 August, the wind speed again was low (3-6 m/s), therefore, the plume was stable and its northern boundary did not cross the point of the mooring station. This location of the plume border is confirmed by cloud-free satellite image acquired on 8 August.

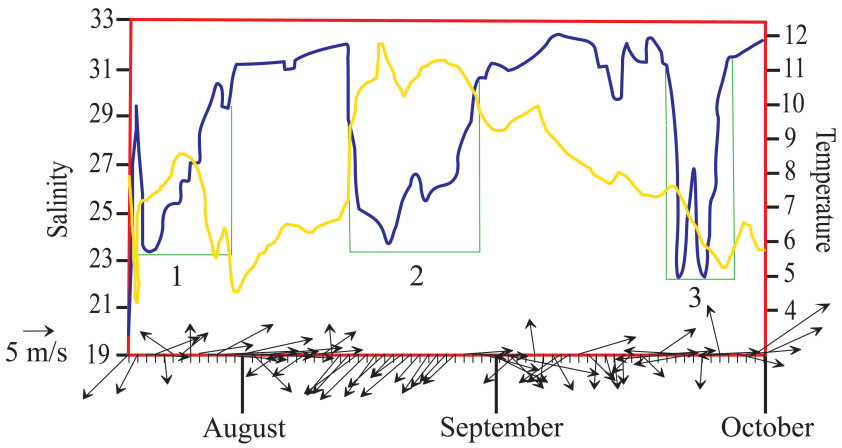

FIGURE 9
Daily temperature (yellow line) and salinity (blue line) measurements in the surface layer on 20 July – 1 October 2002 and the accompanying wind forcing conditions in the Pechora Sea (arrows). Three periods of reduced salinity are indicated by green lines and numbers.

The second period of reduced salinity at the mooring station was observed on 12-30 August (Figure 9). The initial salinity drop was very sharp, it decreased from 32 to 23 in less than a day. This feature could be explained by influence of strong northeastern wind (8-11 m/s), which dominated over the Pechora Sea from 12 to 15 August. Next 10 days northeastern wind remained, albeit with smaller velocities, which was followed by moderate western wind (7 m/s) on 26-29 August and strong western wind (15 m/s) on 30 August. This change in wind forcing resulted in steady increase of surface salinity at the mooring station to 30-33, which occurred from 27 to 30 August.

Wind forcing in the beginning of September was mainly low (< 5 m/s) with variable direction. The Pechora plume was stable during this period and did not spread over the mooring station. Moderate eastern wind (7-8 m/s) on 19-21 September induced northward advection of the Pechora plume indicated by the third period of reduced salinity, which started on 22 September (Figure 9). Southwestern wind (up to 8-14 m/s), which dominated in the end of September, restored the seawater salinity conditions of 31-33 at the mooring station by 27 September.

Satellite imagery regularly demonstrates inflow of warm waters of the Pechora plume to the Kara Sea through the Kara Strait. This process occurs during the periods of large area of the plume forced by southeastern winds. In particular, strong southeastern wind (5-10 m/s), which prevailed over the Pechora Sea on 23-25 July 2020, caused formation of this inflow (Figure 10). In the Kara Sea, the Pechora plume does not propagate far off the Vaygach Island and is mixed with ambient saline seawater. The intense mixing is possibly caused by strong internal waves, which are very frequent in the Kara Strait (Morozov et al., 2003; Morozov et al., 2008; Kozlov et al., 2015a; Morozov et al., 2017).

3.4 Wind-driven upwelling events within the Pechora plume

Analysis of cloud-free and ice-free satellite imagery in June-October 2003-2021 showed regular formation of wind-induced coastal upwelling events within the Pechora plume. The most frequent upwelling events formed under northeastern wind forcing are registered along the Varandey shore and along the Russkiy Zavorot Peninsula (Figure 1). Several examples of typical manifestation of upwelling events at thermal satellite images as coastal stripes of cold water bounded by certain bathymetry isolines are shown in Figure 11. Similar upwelling events visible at satellite imagery within other large river plumes (Lena, Indigirka, and Kolyma plumes) in the Arctic Ocean were reported by Osadchiev et al. (2020c). Regular formation of these events could strongly affect structure of river plumes by intensification of their vertical mixing, especially if upwelling events occur near the river estuaries and deltas (Austin and Lentz, 2002; Lentz and Fewings, 2012; Osadchiev et al., 2020c).

In late July 2017, *in situ* measurements were performed in the Pechora Sea during formation of wind upwelling along the Varandey shore, which allowed us to assess the influence of this event on the Pechora plume (Figure 12). CTD stations during this survey were made near the shore within the upwelling area (cyan color in Figure 12) and at the distance of 20-30 km from the shore off this area (red color in Figure 12). *In situ* measurements demonstrated intense mixing of the Pechora plume during upwelling event, which resulted in increase of surface salinity from 10 to 26, while the plume depth remained stable (5 m).

Common cloud-free conditions in the Pechora Sea in late July and early August 2004 provided opportunity to assess velocity of

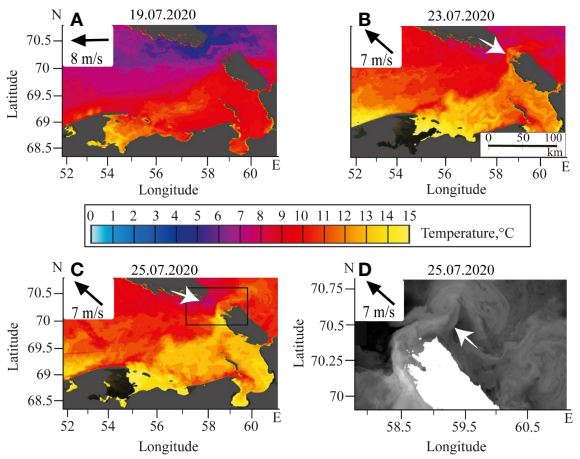

FIGURE 10
Satellite-derived Sea surface temperature in the Pechora Sea on 19 July **(A)**, 23 July **(B)**, 25 July **(C, D)** 2020 acquired by NOAA-20/VIIRS **(A-C)** and Landsat-8 **(D)**. Inflows of the Pechora plume to the Kara Sea through the Kara Strait are indicated by white arrows. Black rectangle in panel **(C)** indicates location of the zoomed area shown in panel **(D)**. Dark grey color at panels **(A-C)** and white color at panel **(D)** indicate land; white color at panels **(A-C)** indicates cloud coverage of the study area. Wind direction and velocity averaged during two days preceding the satellite image are shown in the insets.

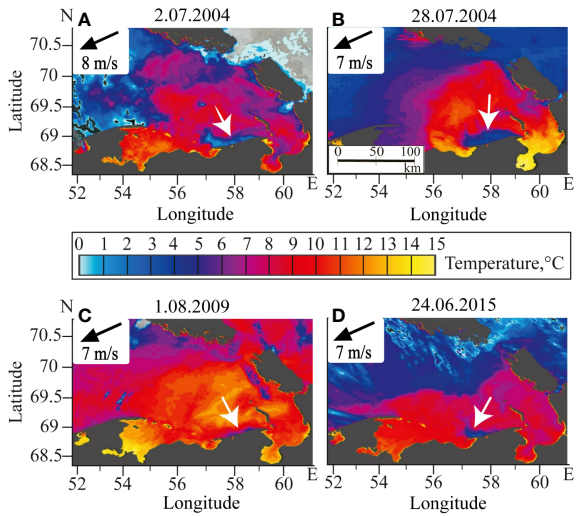

FIGURE 11
Satellite-derived Sea surface temperature in the Pechora Sea on 2 July 2004 **(A)**, 28 July 2004 **(B)**, 1 August 2009 **(C)**, 24 June 2015 **(D)** acquired by MODIS Terra/Aqua. Areas of upwelling events are indicated by white arrows. Dark grey color indicates land; white color indicates cloud coverage of the study area. Wind directions and velocities averaged during two days preceding the satellite image are shown in the insets.

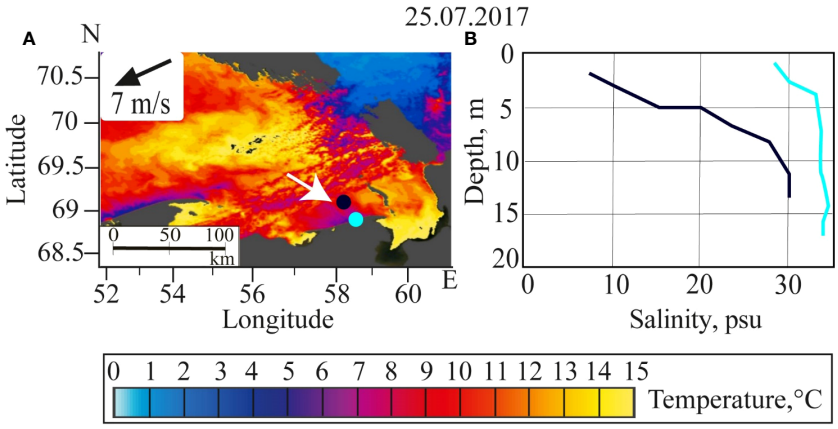

FIGURE 12
Satellite-derived Sea surface temperature in the Pechora Sea on 25 July 2017 acquired by MODIS Terra **(A)** and vertical salinity measurements performed on 26 July 2017 within (cyan color) and outside (black color) the upwelling area **(B)**. Area of upwelling events indicated by white arrow in panel **(A)**. Colored circles indicate locations of the in-situ measurements. Dark grey color indicates land, white color indicates cloud coverage of the study area. Wind direction and velocity averaged during two days preceding the satellite image are shown in the inset.

formation of upwelling area under northeastern wind forcing and its subsequent dissipation after secession of upwelling-favorable winds. Three days of moderate northeastern wind (up to 7 m/s) on 25-26 July caused formation of the primary upwelling area of 400 km^2 visible on 26 July (Figure 13A). Similar upwelling-favorable winds dominated during the next two days, as a result, the upwelling area increased to 1 800 km^2 by 28 July (Figure 13B). During the next two days wind velocity decreased to 2-3 m/s, and the upwelling area started dissipating (Figure 13C). It finally disappeared during the next two days of northern wind forcing and was completely absent on 2 August (Figure 13D).

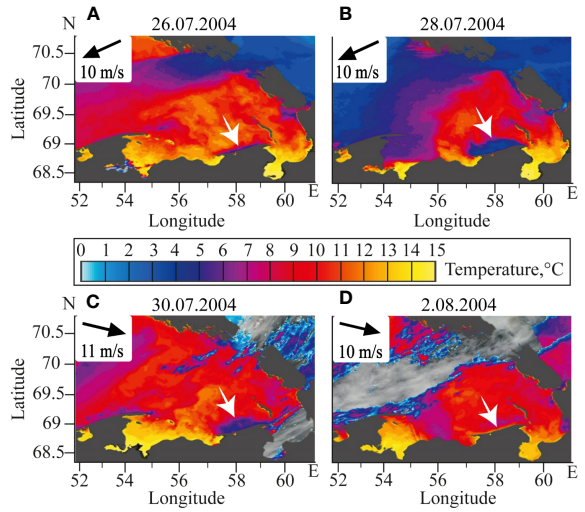

FIGURE 13
Satellite-derived Sea surface temperature in the Pechora Sea on 26 July 2004 **(A)**, 28 July 2004 **(B)**, 30 July 2004 **(C)**, 2 August 2004 **(D)** acquired by MODIS Terra/Aqua. Areas of upwelling events are indicated by white arrows. Dark grey color indicates land, white color indicates cloud coverage of the study area. Wind directions and velocities averaged during two days preceding the satellite image are shown in the insets.

4 Discussion

4.1 Synoptic variability of the Pechora plume

The analyzed *in situ* and satellite data showed that spatial distribution of the Pechora plume has a significant variability on daily and weekly time scales (Table 2). This variability, first, is caused by advection of the plume under wind forcing and the resulting changes in the plume area. We observe that moderate and strong (5-10 m/s) wind forcing with stable direction distinctly modifies plume spreading in 1.5-2 days. The plume area increases with southeastern, eastern, and northeastern winds, which favor plume advection to the open part of the Pechora Sea due to the resulting Ekman transport. Under prevailing southeastern and eastern winds, the Pechora plume occupies the entire area between the Pechora Bay and the Vaygach Island (Figures 7, 8B). Satellite images show that during certain periods the Pechora plume inflows to the Kara Sea through the Kara Strait by a narrow alongshore current and propagates further along the eastern coast of the Vaygach Island (Figure 10). Long-term northeastern winds, on the opposite, could force the Pechora plume to spread westward from the Pechora Bay along the Russkiy Zavorot peninsula (Figures 4A, 7). Western and northwestern winds have the opposite effect. They hinder spreading the Pechora plume of in the open part of the Pechora and, therefore, reduce its area. In such cases, the Pechora plume is arrested within the Pechora Bay and also occupies a narrow stripe (10-20 km) along the Varandey shore (Figures 4C, 7). During periods of weak wind (< 5 m/s) or wind of variable direction, area of the Pechora plume remains stable.

The second important factor of wind influence on the Pechora plume on the synoptic time scale consists in intense mixing of the plume and the underlying seawater that increases salinity of the plume and reduces its area. Wind-induced mixing occurs, first, as a result of direct wind impact on the plume and, second,

TABLE 2 Main information about general spreading types of the Pechora plume.

General spreading types of the Pechora plume	Plume area	Periods of the oceanographic surveys	Key external forcing conditions
Minimal	6 000 - 7 000 km²	July 1993, 1994, 1995, 2019 and August 1998	Drought period; moderate or strong western winds, which press the plume towards the shore, or very strong winds, which induce intense mixing of the plume
Average	20 000 - 22 000 km²	July 2014 and July 2021	Drought period; low or moderate wind forcing
Maximal	25 000 - 36 000 km²	July 2017, 2018 and 2020	Freshet period; moderate or strong northeastern or eastern winds; large ice coverage of the Pechora Sea by the beginning of the freshet period

due to formation of wind upwelling events in the coastal zone. In the first case, more than three days of strong (> 10-12 m/s) wind induce intense mixing of the Pechora plume and its dissipation in the area between the Pechora Bay and the Kolguev Island. As a result, the Pechora plume remains only at the shallow area along then Varandey shore, where it occupies the entire water column from surface to bottom. This process was observed by *in situ* measurements in July 1993 (Figure 7) and by satellite observations in July 2019 (Figure 8C), which was manifested by abrupt southward shift of the plume border and the reduction of the plume area.

The second mechanism of wind-induced plume mixing is formation of upwelling events along the Varandey shore (Figure 11). These events are generated under the influence of moderate (> 6 m/s) northeastern winds. The area of cold and saline upwelling region formed within the Pechora plume steadily increases up to 1700-1800 km^2 during 2-4 days of upwelling-favorable winds and then remains stable (Figure 13). First surface manifestation of upwelling events within the Pechora plume appears after 12 hours of northeastern wind, which is much smaller than the response of spreading dynamics of the Pechora plume to wind variability (1.5-2 days). According to wind reanalysis data, upwellings within the Pechora plume occur predominantly in June and July, however, certain events were observed in August and September. Duration of the majority of upwelling events varies from 2 to 7 days.

Despite wind forcing effects, certain submesoscale processes could affect spreading and mixing of the Pechora plume. In particular, it is highly likely, that strong internal waves in the Kara Strait substantially contribute to mixing of the Pechora plume and could be the main factor, which hinders its further eastward advection to the Kara Sea (Morozov et al., 2003; Morozov et al., 2008; Kozlov et al., 2015a; Morozov et al., 2017). However, the internal waves (Kozlov et al., 2015b) as well as submesoscale eddies (Atadzhanova et al., 2017) are rare in the Pechora Sea and therefore limitedly affect the Pechora plume. Finally, tidal mixing is relatively low in the Pechora Sea (Nikiforov et al., 2005a), albeit it intensifies in the Pechora Bay and could affect initial interaction and mixing of freshwater discharge and seawater in the gulf.

4.2 Seasonal and inter-annual variability of the Pechora plume

Spatial variability of the Pechora plume on seasonal and inter-annual time scales is strongly affected by variability of the Pechora River runoff. The main contribution to the seasonal plume variability is made by the increased volume of the Pechora runoff during the freshet period, which occurs from the end of May till the beginning of July. During the freshet period, up to 70% of the annual river runoff enters the Pechora Sea. As a result, the area of the Pechora plume is large during the freshet period, it occupies the whole area between the Pechora Bay and the Vaygach Island (Figure 7), except short-term periods of intense wind-induced mixing. During the drought period, the area of the Pechora plume decreases to the Pechora Bay and the Varandey shore (Figure 7), except short-term periods of wind-induced northward spreading of the plume.

The inter-annual variability of the volume of the Pechora runoff could reach 80 km^3 (Figure 2), which also has a significant influence on the salinity values in the Pechora Bay and in the Pechora Sea. The difference in salinity values within the plume in the Pechora Bay between years with high and low freshet discharge can reach 5-8 (Figure 5E). The inter-annual variability of ice conditions also affects the plume area in case of intense ice melting during freshet period. Melting of significant volume of sea ice in the Pechora Sea during initial formation of the plume in late spring, significantly contributes large volume of freshwater to the plume and inflates the plume area and volume. These processes were observed in June 2018 and resulted in the largest registered area of the Pechora plume (Figure 7).

The Arctic Ocean is experiencing very significant climate change during the recent decades including rapid increase of air temperature, decline of ice coverage and increase of freshwater discharge (Stroeve and Notz, 2018; Box et al., 2019). Certainly, the Pechora Sea is also affected by these processes. However, the available *in situ* data analyzed in this work is too scarce to assess the decadal climatic trends due to strong seasonal and inter-annual variability of the Pechora plume.

4.3 General types of the Pechora plume spreading

Three general spreading types of the Pechora plume detected in this study are summarized in Figure 14 and Table 2. In case of the first ("minimal") spreading type, the plume occupies the Pechora Bay and propagates eastward along the Varandey shore as a narrow (20-40 km wide) jet (indicated by dark-brown area in Figure 14). The plume boundary in this case corresponds to the isobath of 15 m, the plume area is 6 000 - 7 000 km². "Minimal" spreading type was observed during field surveys in 1993, 1994, 1995, 1998, and 2019 (Figure 4). This plume configuration is formed after the end of the freshet period as a result of reduced river discharge; therefore, it is the most typical for the summer-autumn period. However, this configuration could form during freshet period in case of strong wind forcing and intense mixing of the plume.

In case of the second ("average") spreading type, the Pechora plume occupies the entire eastern part of the Pechora Sea (indicated by light-brown area in Figure 14). In this case, the plume area is 20 000 - 22 000 km², which was observed during field surveys in 2014 and 2021 (Figure 7). "Average" spreading type of the Pechora plume is most typical during and shortly after the freshet in absence of strong wind. During the "average" type, an area of increased salinity could form within the plume along the Varandey shore, which is caused by wind upwellings (indicated by yellow area in Figure 14).

The third ("maximal") spreading type is characterized by the most distant propagation of the plume westward from the Pechora Bay and/or eastward to the Kara Strait and further into the Kara Sea (indicated by red area in Figure 14). In this case, the plume area increases to 25 000 - 36 000 km², and the outer boundary of the plume shifts 40-50 km northward, as compared to the "average" type. "Maximal" spreading type was observed during field surveys in 2017, 2018, and 2020 (Figure 7). This spreading type is formed during freshet and is accompanied by moderate eastern and northeastern winds (July 2017 and 2020) and/or intense sea ice melting (June 2018). Finally, we want to highlight that the Pechora plume experiences multiple transitions between all three spreading types during one year due to its quick response to synoptic wind variability.

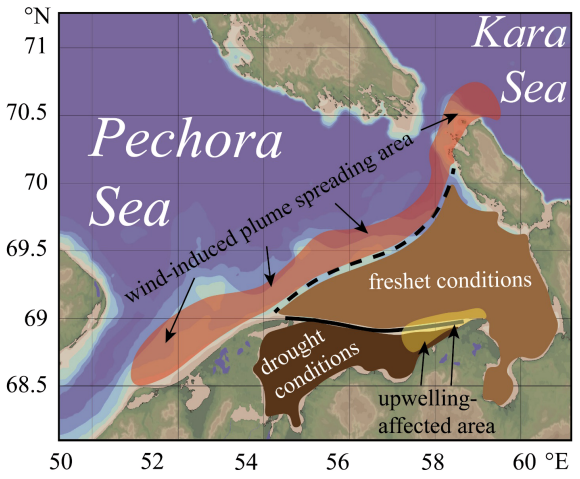

FIGURE 14
Location of the Pechora River plume during drought (dark-brown color) and freshet (light-brown color) conditions, which illustrates seasonal variability of the plume. Wind-induced plume spreading area (red color) and coastal upwelling area (yellow color), which illustrate synoptic variability of the plume.

5 Conclusions

In this work, we analyze the extensive *in situ* data and satellite images collected in the southeastern part of the Barents Sea (also called the Pechora Sea) during ice-free periods. Based on this data, we provide the detailed description of structure and variability of the large Pechora plume formed by the Pechora River discharge. We assess the influence of the main external factors, namely, river discharge rate, local wind forcing, and ice conditions, on spreading of the Pechora plume on synoptic, seasonal, and inter-annual time scales.

The Pechora plume occupies a large area in the Pechora Sea, which varies from 6 000 to 36 000 km^2. The vertical scale of the Pechora plume, in contrast to its area, is rather stable and varies from 4 to 7 m. Sharp salinity gradients are formed between the Pechora plume (with salinities of 2-25) and ambient seawater (30-33). Both horizontal and vertical gradients generally correspond to the isohaline of 25, which is regarded as the outer border of the Pechora plume (similarly to other large river plumes in the Arctic Ocean). Temperatures within the Pechora plume (9-10°C) are higher than those in the ambient sea (5-6°C) in spring and summer, which results in sharp temperature gradient at the plume border. Due to this difference, the Pechora plume is distinctly visible on thermal satellite imagery during cloud-free periods in spring and summer. However, atmospheric cooling in autumn erodes this temperature gradient.

Seasonal variability of the Pechora plume is governed by variability of the Pechora River runoff. The maximal area of the Pechora plume is observed during the freshet period from late May to late July. During this period, the plume occupies the southern and southeastern parts of the Pechora Sea from the Pechora Bay and the Russkiy Zavorot peninsula in the west to the Vaygach Island and the Kara Strait in the east. The zonal and meridional extents of the plume in this case are about 250 and 150 km, respectively. Inter-annual variability of ice conditions in the Pechora Sea also strongly affects spatial characteristics of the Pechora plume. Presence of large ice fields in the southeastern part of the Pechora Sea during the freshet period, which occurs in certain years, results in large fluxes of melt water to the plume. This processes significantly increases volume and area of the plume. The minimal area of the Pechora plume is observed during the drought period in late summer and autumn. During this period, the plume is localized within the Pechora Bay and propagates eastward as a narrow stripe (150 km long and up to 40 km wide) along the Varandey shore.

Wind forcing plays a key role in variability of spatial structure of the Pechora plume on the synoptic time scale. The plume area is increased by moderate (> 5 m/s) eastern, southeastern, and southern winds, but is decreased by northern and northwestern winds due to the resulting Ekman transport. It takes only 1.5-2 days of stable wind forcing to significantly shift the plume border and change the plume area. Such a small response time of the Pechora plume to wind variability also results in its intense mixing with subjacent saline seawater in response to strong (> 10-12 m/s) and durable (> 3 days)

wind of any direction. As a result, during periods of strong winds the area of the Pechora plume could reduce from 30 000 - 36 000 km^2 to 6 000 - 7 000 km^2 in a few days. Under wind influence, the Pechora plume is periodically advected beyond its typical spreading area. In particular, eastern winds could result in westward alongshore (30-40 km) spreading of the plume from the Pechora Bay. Northeastern winds during the periods of large area of the plume cause its regular advection into the Kara Sea through the Kara Strait. However, the Pechora plume was registered only 20-40 km to the east from the Kara Strait and do not merge with the Ob-Yenisei plume. Another important factor inducing intense mixing of the Pechora plume is formation of coastal upwelling events. Upwelling forms within the plume along the Varandey shore after 8-12 hours of moderate (> 6 m/s) northeastern winds, the resulting coastal stripe of saline and cold water within the plume is up to 1 800 km^2.

The study of the Pechora plume is important for understanding different physical, biological, and geochemical processes in the Pechora Sea. In particular, the low-saline plume water directly affects the whole Pechora Sea ecosystem including plankton communities (especially zooplankton), which strongly depend on variability of temperature and salinity in the Pechora Sea (Musaeva and Suntsov, 2001; Usov et al., 2019). Benthic communities, being a part of foodbase of marine mammals, are also affected by local salinity fluctuations (Denisenko et al, 2019b; Dgebuadze et al., 2021; Gebruk et al., 2019; Gebruk et al., 2021; Gebruk et al., 2022; Gebruk et al., 2023). Moreover, spreading and mixing of the Pechora plume determines ice formation and ice melting in the Pechora Sea, which monitoring and forecasting is especially important for the intense marine shipping and fishery in the Pechora Sea (Semushin et al., 2019; Sukhotin et al., 2019). Finally, we want to highlight the increased oil drilling activity in the study area, which requires operational oceanographic support of the Prirazlomnaya offshore stationary platform and the Varandey offshore oil terminal located in the Pechora Sea (Ogorodov, 2005; Nesic et al., 2018).

Despite the certain importance of this study for understanding regional processes in the Pechora Sea, it could be considered in broader context to widen its applicability to other river plumes in the World Ocean. The obtained results improve our understanding of dependence between velocity of plume response to wind variability on the one hand and plume spatial scales on the other hand. The response rate of the Pechora plume to variability of wind forcing is significantly lower than that of the large river plumes. The related temporal scale for the Amazon (Lentz, 1995; Paluszkiewicz et al., 1995; Molleri et al., 2010), Congo (Hopkins et al., 2013), Ob-Yenisei (Osadchiev et al., 2020a; Osadchiev et al., 2021a), Lena (Osadchiev et al., 2021b), Mississippi (Walker, 1996; Walker et al., 2005; Silva and Castelao, 2018) plumes is 2-3 weeks or more. This feature could be explained by smaller depth (4-8 m) and area (6 000 – 36 000 km^2) of the Pechora plume as compared to large river plumes mentioned above (with depths >10 m and areas >100 000 km^2). On the other hand, the response rate of small river plumes with depths of 1-2 m and area of 1-10 km^2 is equal to several hours (Pinones et al., 2005; Korotkina et al., 2011; Korotkina et al., 2014; Qu and Hetland, 2019; Osadchiev et al., 2020d; Osadchiev et al., 2021d), which is much smaller than that for the Pechora plume. We want to highlight, that these results were obtained using *in situ* and satellite data and should be considered for numerical modeling of these river plumes.

Data availability statement

The original contributions presented in the study are included in the article/Supplementary Material. Further inquiries can be directed to the corresponding author.

Author contributions

VR and AO designed the study. VR, AO and OK processed the *in situ* data and organized the database. VR and AO performed the analysis of the *in situ* and satellite data. All authors contributed to manuscript revision, read, and approved the submitted version.

Funding

This research was funded by the Ministry of Science and Higher Education of the Russian Federation, theme FMWE-2021-0001 (collecting and processing of *in situ* and satellite data) and the Russian Science Foundation, research project 22-77-10004 (study of water exchange in the Pechora Sea).

Acknowledgments

The authors wish to thank the crew of R/V “Kartesh” and colleagues from Marine Research Center at Lomonosov Moscow State University for providing *in situ* measurements in 2017-2021. Authors also wish to thank Ekaterina Kuskova from Lomonosov Moscow State University for support in this study.

Conflict of interest

The authors declare that the research was conducted in the absence of any commercial or financial relationships that could be construed as a potential conflict of interest.

Publisher’s note

All claims expressed in this article are solely those of the authors and do not necessarily represent those of their affiliated organizations, or those of the publisher, the editors and the reviewers. Any product that may be evaluated in this article, or claim that may be made by its manufacturer, is not guaranteed or endorsed by the publisher.

Supplementary material

The Supplementary Material for this article can be found online at: https://www.frontiersin.org/articles/10.3389/fmars.2023.1052044/full#supplementary-material

References

Adrov, N. M., and Denisenko, S. G. (1996). "Oceanographic characteristics of the Pechora Sea," in *Biogeocenoses of glacial shelf of the western Arctic seas*. Eds. G. G. Matishov, G. A. Tarasov, S. G. Denisenko, V. V. Denisov and K. V. Galaktionov (Russia: Kola Branch of the Russian Academy of Sciences), 166–179.

Arthun, M., Ingvaldsen, R. B., Smedsrud, L. H., and Schrum, C. (2011). Dense water formation and circulation in the Barents Sea. deep-Sea res. *I: Oceanogr. Res. Pap.* 58 (8), 801–817. doi: 10.1016/j.dsr.2011.06.001

Atadzhanova, O. A., Zimin, A. V., Romanenkov, D. A., and Kozlov, I. E. (2017). Satellite radar observations of small eddies in the White, Barents and Kara Seas. *Phys. Oceanogr.* 2, 75–83. doi: 10.22449/1573-160X-2017-2-75-83

Austin, J. A., and Lentz, S. J. (2002). The inner shelf response to wind-driven upwelling and downwelling. *J. Phys. Oceanogr.* 32 (7), 2171–2193. doi: 10.1175/15200485(2002)032%3C2171:TISRTW%3E2.0.CO;2

Boitsov, V. D., Karsakov, A. L., and Trofimov, A. G. (2012). Atlantic Water temperature and climate in the Barents Sea 200–2009. *ICES J. Mar. Sci.* 69 (5), 833–840. doi: 10.1093/icesjms/fss075

Box, J. E., Colgan, W. T., Christensen, T. R., Schmidt, N. M., Lund, M., Parmentier, F.-J. W., et al. (2019). Key indicators of Arctic climate change: 1971-2017. *Environ. Res. Lett.* 14, 045010. doi: 10.1088/1748-9326/aafc1b

Boyer, T. P., Baranova, O. K., Coleman, C., Garcia, H. E., Grodsky, A., Locarnini, R. A., et al. (2018). "World Ocean database 2018," in *NOAA Atlas NESDIS 87*. Eds. S. Levitus and A. V. Mishonov (USA: Silver Spring).

Byshev, V. I., Galerkin, L. I., and Grotov, A. S. (2001). "Hydrological conditions in the southeastern part of the Barents Sea in august," in *Experience of system oceanologic studies in the Arctic*. Eds. E. A. Romankevich and A. P. Lisitzin (Russia: Scientific World), 85–92.

Dahle, S., Denisenko, S. G., Denisenko, N. V., and Cochrane, S. J. (1998). Benthic fauna in the Pechora Sea. *Sarsia* 83 (3), 183–210. doi: 10.1080/00364827.1998.10413681

Dankers, R., and Middelkoop, H. (2008). River discharge and freshwater runoff to the Barents Sea under present and future climate conditions. *Clim. Change* 87 (1), 131–153. doi: 10.1007/s10584-007-9349-x

Denisenko, N. V., Denisenko, S. G., and Lehtonen, K. K. (2019a). Distribution of macrozoobenthos in an Arctic estuary (Pechora Bay, SE Barents Sea) during the spring flood period. *Polar Biol.* 42 (9), 1667–1684. doi: 10.1007/s00300-018-02452-6

Denisenko, S. G., Denisenko, N. V., Chaban, E. M., Gagaev, S. Y., Petryashov, V. V., Zhuravleva, N. E., et al. (2019b). The current status of the macrozoobenthos around the Atlantic walrus haul-outs in the Pechora Sea (SE Barents Sea). *Polar Biol.* 42 (9), 1703–1717. doi: 10.1007/s00300-018-02455-3

Denisenko, S. G., Denisenko, N. V., Lehtonen, K. K., Andersin, A. B., and Laine, A. O. (2003). Macrozoobenthos of the Pechora Sea (SE Barents Sea): Community structure and spatial distribution in relation to environmental conditions. *Mar. Ecol. Progr. Ser.* 258, 109–123. doi: 10.3354/meps258109

Denisenko, S. G., Sandler, H., Denisenko, N., and Rachor, E. (2000). Current state of zoobenthos in two estuarine bays of the Barents and Kara Seas. *ICES J. Mar. Sci.* 56, 187–193. doi: 10.1006/jmsc.1999.0633

Dgebuadze, P. Y., Basin, A. B., Chikina, M. V., Udalov, A. A., Balakin, A. A., Razgon, I. L., et al. (2021). Transformation of benthic communities in Pechora Bay and the probable loss of the portlandia aestuariorum population in the typical habitat. *Oceanology* 61 (6), 976–983. doi: 10.1134/S0001437021060059

Drinkwater, K. F. (2011). The influence of climate variability and change on the ecosystems of the Barents Sea and adjacent waters: Review and synthesis of recent studies from the NESSAS project. *Progr. Oceanogr.* 90 (1-4), 47–61. doi: 10.1016/j.pocean.2011.02.006

Dvoretsky, V. G., and Dvoretsky, A. G. (2013). Structure of mesozooplankton community in the Barents Sea and adjacent waters in august 2009. *J. Natur. Hist.* 47 (31-32), 2095–2114. doi: 10.1080/00222933.2013.772670

Frey, D. I., and Osadchiev, A. A. (2021). Large river plumes detection by satellite altimetry: Case study of the Ob–Yenisei plume. *Rem. Sen.* 13 (24), 5014. doi: 10.3390/rs13245014

Gebruk, A. A., Borisova, P. B., Glebova, M. A., Basin, A. B., Simakov, M. I., Shabalin, N. V., et al. (2019). Macrozoobenthos of the shallow waters of Pechora Bay (SE Barents Sea). *Nat. Conserv. Res.* 4 (4), 1–11. doi: 10.24189/ncr.2019.058

Gebruk, A., Dgebuadze, P., Rogozhin, V., Yu., E., Shabalin, N., and Mokievsky, V. (2023). Macrozoobenthos of the Pechora Bay in 2020-2021 indicates a likely change in common bivalve molluscs in the Arctic estuary. *Polar Biol.* in press.

Gebruk, A., Ermilova, Y., Henry, L. A., Henley, S. F., Spiridonov, V., Shabalin, N., et al. (2022). "Microplastics in the Arctic benthic fauna: A case study of the snow crab in the Pechora Sea, Russia," in *Building common interests in the Arctic ocean with global inclusion*, Ed. P. A. Berkman, et al (Germany: Springer) 2, 85–102. doi: 10.1007/978-3-030-89312-5_685

Gebruk, A., Mikhaylyukova, P., Mardashova, M., Semenova, V., Henry, L. A., Shabalin, N., et al. (2021). Integrated study of benthic foraging resources for Atlantic walrus (Odobenus rosmarus rosmarus) in the Pechora Sea, south-eastern Barents Sea. *Aquat. Conserv. Mar. Freshw. Ecosyst.* 31 (1), 112–125. doi: 10.1002/aqc.3418

Gerasimova, A. V., Filippova, N. A., Lisitsyna, K. N., Filippov, A. A., Nikishina, D. A., and Maximovich, N. V. (2019). Distribution and growth of bivalve molluscs serripes groenlandicus (Mohr) and macoma calcarea (Gmelin) in the Pechora Sea. *Polar Biol.* 42, 1685–1702. doi: 10.1007/s00300-019-02550-z

Gordeev, V. V., Martin, J. M., Sidorov, I. S., and Sidorova, M. V. (1996). A reassessment of the Eurasian river input of water, sediment, major elements, and nutrients to the Arctic Ocean. *Am. J. Sci.* 296 (6), 664–691. doi: 10.2475/ajs.296.6.664

Haine, T. W., Curry, B., Gerdes, R., Hansen, E., Karcher, M., Lee, C., et al. (2015). Arctic freshwater export: Status, mechanisms, and prospects. *Glob. Planet. Change* 125, 13–35. doi: 10.1016/j.gloplacha.2014.11.013

Hopkins, J., Lucas, M., Dufau, C., Sutton, M., Stum, J., Lauret, O., et al. (2013). Detection and variability of the Congo river plume from satellite derived sea surface temperature, salinity, ocean colour and sea level. *Remote Sens. Environ.* 139), 365–385. doi: 10.1016/j.rse.2013.08.015

Ilyin, G. V., and Matishov, G. G. (1992). "Oceanographic conditions in the Pechora Sea in July," in *An international American-Norwegian-Russian ecological expedition in the Pechora Sea, Novaya zemlya, Zaygach, Kolguyev and Dolgiy islands, July 1992 (RV 'Dalnie zelentzy'), MMBI report*. Ed. G. G. Matishov (Russia: Kola Branch of the Russian Academy of Sciences) 7–11.

Jakobsson, M., Mayer, L. A., Coakley, B., Dowdeswell, J. A., Forbes, S., Fridman, B., et al. (2012). The international bathymetric chart of the Arctic Ocean (IBCAO), version 3.0. *Geophys. Res. Lett.* 39 (12), L12609. doi: 10.1029/2012gl052219

Korotkina, O.A., Zavialov, P. O., and Osadchiev, A.A. (2011). Submesoscale variability of the current and wind fields in the coastal region of Sochi. *Oceanology* 51 (5), 745–754. doi: 10.1134/s0001437011050109

Korotkina, O.A., Zavialov, P.O., and Osadchiev, A.A. (2014). Synoptic variability of currents in the coastal waters of Sochi. *Oceanology* 54 (5), 545–556. doi: 10.1134/s0001437014040079

Kozlov, I. E., Kudryavtsev, V. N., Zubkova, E. V., Zimin, A. V., and Chapron, B. (2015a). Characteristics of short-period internal waves in the Kara Sea inferred from satellite SAR data. *Izv. Atm. Ocean. Phys.* 51 (9), 1073–1087. doi: 10.1134/S0001433815090121

Kozlov, I. E., Kudryavtsev, V. N., Zubkova, E. V., Atadzhanova, O. A., Zimin, A. V., Romanenkov, D., et al. (2015b). SAR observations of internal waves in the Russian Arctic seas. *IEEE Int. Geosci. Rem. Sens. Symp. (IGARSS)* 2015, 947–949. doi: 10.1109/IGARSS.2015.7325923

Kurtz, N. T., and Markus, T. (2012). Satellite observations of Antarctic sea ice thickness and volume. *J. Geophys. Res. Oceans* 117, C08025. doi: 10.1029/2012JC008141

Lee, K.-H., Chung, K.-H., Soh, H.-Y., and Lee, W. (2003). On the distribution of zooplankton in the southeastern Barents Sea during July 2002. *Korean J. Environ. Biol.* 21 (4), 392–399.

Lentz, S. J. (1995). The Amazon river plume during AMASSEDS: subtidal current variability and the importance of wind forcing. *J. Geophys. Res. Oceans* 100 (2), 2377–2390. doi: 10.1029/94JC00343

Lentz, S. J., and Fewings, M. R. (2012). The wind- and wave-driven inner-shelf circulation. *Ann. Rev. Mar. Sci.* 4, 317–343. doi: 10.1146/annurev-marine-120709-142745

Lind, S., Ingvaldsen, R. B., and Furevik, T. (2018). Arctic warming hotspot in the northern Barents Sea linked to declining sea-ice import. *Nat. Clim. Change* 8 (7), 634–639. doi: 10.1038/s41558-018-0205-y

Liu, Z., Risi, C., Codron, F., Jian, Z., Wei, Z., He, X., et al. (2022). Atmospheric forcing dominates winter Barents-Kara Sea ice variability on interannual to decadal time scales. *Proc. Nat. Acad. Sci.* 119 (36), e2120770119. doi: 10.1073/pnas.2120770119

Loeng, H. (1991). Features of the physical oceanographic conditions of the Barents Sea. *Polar Res.* 10 (1), 5–18. doi: 10.3402/polar.v10i1.6723

Loeng, H., Ozhigin, V., and Ådlandsvik, B. (1997). Water fluxes through the Barents Sea. *ICES J. Mar. Sci.* 54 (3), 310–317. doi: 10.1006/jmsc.1996.0165

Magritsky, D., Lebedeva, S., and Skripnik, E. (2017). Hydrological hazards at mouths of the Northern Dvina and the Pechora Rivers, Russian Federation. *Nat. Haz.* 88 (1), 149–170. doi: 10.1007/s11069-016-2673-6

Mokhova, O. N., Melnik., R. A., and Bolotov, I. N. (2019). "Variability of hydrological and hydrochemical characteristics in the Pechora Bay of the Barents Sea," in *Problems of ecological safety and sustainable development of Arctic research* (Russia: Arctic Research Center of the Russian Academy of Sciences).

Molleri, G. S., Novo, E. M. D. M., and Kampel, M. (2010). Space-time variability of the Amazon river plume based on satellite ocean color. *Cont. Shelf Res.* 30 (3-4), 342–352. doi: 10.1016/j.csr.2009.11.015

Morozov, E. G., Kozlov, I. E., Shchuka, S. A., and Frey, D. I. (2017). Internal tide in the Kara Gates Strait. *Oceanology* 57 (1), 8–18. doi: 10.1134/S0001437017010106

Morozov, E. G., Paka, V. T., and Bakhanov, V. V. (2008). Strong internal tides in the Kara Gates Strait. *Geophys. Res. Lett.* 35, L16603. doi: 10.1029/2008GL033804

Morozov, E. G., Parrilla-Barrera, G., Velarde, M. G., and Scherbinin, A. D. (2003). The straits of Gibraltar and Kara Gates: A comparison of internal tides. *Oceanol. Acta* 26 (3), 231–241. doi: 10.1016/S0399-1784(03)00023-9

Mu, L., Yang, Q., Losch, M., Losa, S. N., Ricker, R., Nerger, L., et al. (2018a). Improving sea ice thickness estimates by assimilating CryoSat-2 and SMOS sea ice thickness data simultaneously. *Q. J. R. Meteorol. Soc* 144 (711), 529–538. doi: 10.1002/qj.3225

Mu, L., Losch, M., Yang, Q., Ricker, R., Losa, S. N., and Nerger, L. (2018b). Arctic-wide sea ice thickness estimates from combining satellite remote sensing data and a dynamic ice-ocean model with data assimilation during the CryoSat-2 period. *J. Geophys. Res. Oceans* 123, 7763–7780. doi: 10.1029/2018JC014316

Musaeva, E. I., and Suntsov, A. V. (2001). On the distribution of the Pechora Sea zooplankton (On the materials collected in august 1998). *Oceanology* 41 (4), 508–516.

Nesic, S., Pivovarov, K., Streletskaya, V., and Zolotukhin, A. (2018). Mapping the main risks for offshore operations in the Pechora Sea. *WIT Trans. Built Environ.* 174, 69–80. doi: 10.2495/SAFE170071

Nikiforov, S. L., Dunaev, N. N., and Politova, N. V. (2005a). "Modern environmental conditions of the Pechora Sea (climate, currents, waves, ice regime, tides, river runoff, and geological structure," in *Pechora Sea environments: past, present and future*. Eds. H. A. Bauch, Pavlidis,, A. Yu., I. Polyakove Ye., G. G. Matishov and N. Koc (Germany: Ber. Polarforsch. Meeresforsch), 7–38.

Nikiforov, S. L., Pavlidis, Y. A., Rachold, V., Grigoryev, M. N., Rivkin, F. M., Ivanova, N. V., et al. (2005b). Morphogenetic classification of the Arctic coastal zone. *Geo-Mar. Lett.* 25 (2), 89–97. doi: 10.1007/s00367-004-0190-1

Ogorodov, S. A. (2005). Human impacts on coastal stability in the Pechora Sea. *Geo-Mar. Lett.* 25, 190–195. doi: 10.1007/s00367-004-0200-3

Osadchiev, A. A. (2017). Spreading of the Amur river plume in the Amur Liman, the Sakhalin Gulf, and the Strait of Tartary. *Oceanology* 57 (3), 376–382. doi: 10.1134/S0001437017020151

Osadchiev, A. A. (2021). Spreading and transformation of river discharge in the Arctic Ocean. *Herald Russ. Acad. Sci.* 91 (6), 694–699. doi: 10.1134/S1019331621060101

Osadchiev, A. A., Asadulin, E. E., Miroshnikov, A., Zavialov, I. B., Dubinina, E. O., and Belyakova, P. A. (2019). Bottom sediments reveal inter-annual variability of interaction between the Ob and Yenisei Plumes in the Kara Sea. *Sci. Rep.* 9, 18642. doi: 10.1038/s41598-019-55242-3

Osadchiev, A.A., Barymova, A.A., Sedakov, R. O., Rybin, A. V., Tanurkov, A.G., Krylov, A.A., et al. (2020d). Hydrophysical structure and current dynamics of the Kodor river plume. *Oceanology* 61 (1), 1–14. doi: 10.1134/S000143702101015X

Osadchiev, A. A., Frey, D. I., Shchuka, S. A., Tilinina, N. D., Morozov, E. G., and Zavialov, P. O. (2021a). Structure of the freshened surface layer in the Kara Sea during ice-free periods. *J. Geophys. Res. Oceans* 126 (1), e2020JC016486. doi: 10.1029/2020JC016486

Osadchiev, A. A., Frey, D. I., Spivak, E. A., Shchuka, S. A., Tilinina, N. D., and Semiletov, I. P. (2021b). Structure and inter-annual variability of the freshened surface layer in the Laptev and East-Siberian seas during ice-free periods. *Front. Mar. Sci.* 8. doi: 10.3389/fmars.2021.735011

Osadchiev, A. A., Izhitskiy, A. S., Zavialov, P. O., Kremenetskiy, V. V., Polukhin, A. A., Pelevin, V. V., et al. (2017). Structure of the buoyant plume formed by Ob and Yenisei river discharge in the southern part of the Kara Sea during summer and autumn. *J. Geophys. Res. Oceans* 122 (7), 5916–5935. doi: 10.1002/2016JC012603

Osadchiev, A. A., Konovalova, O. P., and Gordey, A. S. (2021c). Water exchange between the Gulf of Ob and the Kara Sea during ice-free seasons: The roles of river discharge and wind forcing. *Front. Mar. Sci.* 8. doi: 10.3389/fmars.2021.741143

Osadchiev, A. A., Medvedev, I. P., Shchuka, S. A., Kulikov, M. E., Spivak, E. A., Pisareva, M. A., et al. (2020b). Influence of estuarine tidal mixing on structure and spatial scales of large river plumes. *Ocean Sci.* 16 (4), 781–798. doi: 10.5194/os-16-781-2020

Osadchiev, A. A., Pisareva, M. N., Spivak, E. A., Shchuka, S. A., and Semiletov, I. P. (2020a). Freshwater transport between the Kara, Laptev, and East-Siberian seas. *Sci. Rep.* 10, 13041. doi: 10.1038/s41598-020-70096-w

Osadchiev, A. A., Sedakov, R. O., and Barymova, A.A. (2021d). Response of a small river plume on wind forcing. *Front. Mar. Sci.* 8. doi: 10.3389/fmars.2021.809566

Osadchiev, A. A., Silvestrova, K. P., and Myslenkov, S. A. (2020c). Wind-driven coastal upwelling near large river deltas in the Laptev and East-Siberian seas. *Rem. Sen.* 12 (5), 844. doi: 10.3390/rs12050844

Osadchiev, A. A., and Zavialov, P. O. (2020). "Structure and dynamics of plumes generated by small rivers," in *Estuaries and Coastal Zones - Dynamics and Response to Environmental Changes*, ed. J. Pan (London: IntechOpen).

Paluszkiewicz, T., Curtin, T. B., and Chao, S. Y. (1995). Wind-driven variability of the Amazon river plume on the continental shelf during the peak outflow season. *Geomar. Lett.* 15 (3), 179–184. doi: 10.1007/BF01204461

Pinones, A., Valle-Levinson, A., Narváez, D. A., Vargas, C. A., Navarrete, S. A., Yuras, G., et al. (2005). Wind-induced diurnal variability in river plume motion. *Estuar. Coast. Shelf Sci.* 65 (3), 513–525. doi: 10.1016/j.ecss.2005.06.016

Polonsky, V. F. (2012). Influence of tides on the redistribution of water flow in the delta of the Pechora River. *Arctic Ecol. Econ.* 2 (6), 20–27.

Qu, L., and Hetland, R. D. (2019). Temporal resolution of wind forcing required for river plume simulations. *J. Geophys. Res. Oceans* 124 (3), 1459–1473. doi: 10.1029/2018JC014593

Saha, S., Moorthi, S., Pan, H.-L., Wu, X., Wang, J., Nadiga, S., et al. (2010). The NCEP climate forecast system reanalysis. *Bull. Amer. Meteor. Soc* 91, 1015–1057. doi: 10.1175/2010BAMS3001.1

Saha, S., Moorthi, S., Wu, X., Wang, J., Nadiga, S., Tripp, P., et al. (2014). The NCEP climate forecast system version 2. *J. Clim.* 27, 2185–2208. doi: 10.1175/JCLI-D-12-00823.1

Semushin, A. V., Novoselov, A. P., Sherstkov, V. S., Levitsky, A. L., and Novikova, Y. V. (2019). Long-term changes in the ichthyofauna of the Pechora Sea in response to ocean warming. *Polar Biol.* 42 (9), 1739–1751. doi: 10.1007/s00300-018-2405-3

Silva, C. E., and Castelao, R. M. (2018). Mississippi River plume variability in the Gulf of Mexico from SMAP and MODIS-aqua observations. *J. Geophys. Res. Oceans* 123 (9), 6620–6638. doi: 10.1029/2018JC014159

Skagseth, Ø., Drinkwater, K. F., and Terrile, E. (2011). Wind-and buoyancy-induced transport of the Norwegian Coastal Current in the Barents Sea. *J. Geophys. Res. Oceans* 116, C08007. doi: 10.1029/2011JC006996

Skagseth, Ø., Eldevik, T., Årthun, M., Asbjørnsen, H., Lien, V. S., and Smedsrud, L. H. (2020). Reduced efficiency of the Barents Sea cooling machine. *Nat. Clim. Change* 10 (7), 661–666. doi: 10.1038/s41558-020-0772-6

Smedsrud, L. H., Esau, I., Ingvaldsen, R. B., Eldevik, T., Haugan, P. M., Li, C., et al. (2013). The role of the Barents Sea in the Arctic climate system. *Rev. Geophys.* 51 (3), 415–449. doi: 10.1002/rog.20017

Smedsrud, L. H., Ingvaldsen, R., Nilsen, J. E., and Skagseth, Ø. (2010). Heat in the Barents Sea: Transport, storage, and surface fluxes. *Ocean Sci.* 6 (1), 219–234. doi: 10.5194/os-6-219-2010

Spivak, E. A., Osadchiev, A. A., and Semiletov, I. P. (2021). Structure and variability of the Lena river plume in the south-eastern part of the Laptev Sea. *Oceanology* 61 (6), 839–849. doi: 10.1134/S00014370210601

Stroeve, J., and Notz, D. (2018). Changing state of Arctic sea ice across all seasons. *Environ. Res. Lett.* 13, 103001. doi: 10.1088/1748-9326/aade56

Sukhotin, A., Denisenko, S., and Galaktionov, K. (2019). Pechora Sea ecosystems: current state and future challenges. *Polar Biol.* 42 (9), 1631–1645. doi: 10.1007/s00300-019-02553-w

Usov, N., Khaitov, V., Smirnov, V., and Sukhotin, A. (2019). Spatial and temporal variation of hydrological characteristics and zooplankton community composition influenced by freshwater runoff in the shallow Pechora Sea. *Polar Biol.* 42 (9), 1647–1665. doi: 10.1007/s00300-018-2407-1

Vedernikov, V. I., Gagarin, V. I., and Burenkov, V. I. (2001). Features of distribution of primary production and chlorophyll in the Pechora Sea in August-September 1998. *Oceanology* 41 (1), 64–74.

Walker, N. D. (1996). Satellite assessment of Mississippi river plume variability: causes and predictability. *Remote Sens. Environ.* 58 (1), 21–35. doi: 10.1016/0034-4257(95)00259-6

Walker, N. D., Wiseman, W. J.Jr, Rouse, L. J.Jr, and Babin, A. (2005). Effects of river discharge, wind stress, and slope eddies on circulation and the satellite-observed structure of the Mississippi river plume. *J. Coast. Res.* 21 (6), 1228–1244. doi: 10.2112/04-0347.1

Zabolotskikh, E. V., and Balashova, E. A. (2021). External calibration of MTVZA-GYa microwave radiometer measurements in scanner channels. part 2. the experiment. *Russ. Met. Hydrol.* 46 (11), 755–761. doi: 10.52002/0130-2906-2021-11-47-55

Zavialov, I. B., Osadchiev, A. A., Sedakov, R. O., Barnier, B., Molines, J.-M., and Belokopytov, V. N. (2020). Water exchange between the Sea of Azov and the Black Sea through the Kerch Strait. *Ocean Sci.* 16, 15–30. doi: 10.5194/os-16-15-2020